Emerging Materials Research
Volume 1 Issue EMR2
Thermal boundary conductance of transition metals on diamond
Monachon and Weber

ice | science

Pages 89–98 http://dx.doi.org/10.1680/emr.11.00011
Themed Issue Paper
Received 14/10/2011 Accepted 06/01/2012
Published online 13/01/2012
Keywords: time-domain thermoreflectance/thermal boundary conductance/metals/diamond interface

ice Institution of Civil Engineers publishing

Thermal boundary conductance of transition metals on diamond

Christian Monachon MEng
Laboratory of Mechanical Metallurgy, Institute of Materials, Ecole Polytechnique Fédérale de Lausanne (EPFL), Lausanne, Switzerland

Ludger Weber PhD
Laboratory of Mechanical Metallurgy, Institute of Materials, Ecole Polytechnique Fédérale de Lausanne (EPFL), Lausanne, Switzerland

An experimental process that was used to obtain a direct measurement of thermal boundary conductance (TBC) between a diamond substrate and several transition metals, deposited by sputtering, is described. Using time-domain thermoreflectance (TDTR), the critical parameters, for a proper interpretation of the results, are evaluated to be the laser spot size and the thickness of the metallic thin films. Values of TBC between Cu, Cr, Nb, Mo, W and diamond are presented and vary between 30 and 280 MW/m²/K. The adhesion of the layer to the substrate is seen to be critical to obtain a high TBC. Annealing in vacuum at temperatures up to 600°C does not significantly seem to change the results obtained. When diamond surface is oxygen plasma treated for better adhesion, the TBC between Cr and diamond is measured to be 325 MW/m²/K.This represents an 11-fold increase compared to untreated diamond.

List of notations

$C_{v:}$ the volumetric heat capacity of the metal [Jm-3K-1]
d: metallic layer thickness [nm]
G: Thermal boundary conductance [Wm-2K-1]
J: heat flux [Wm-2]
S: sensitivity parameter
X: in phase output of lock in amplifier
Y: out-of-phase output of lock in amplifier
ΔT_{int}: interfacial temperature drop [K]
κ: thermal conductivity [Wm-1K-1]

1. Introduction

In recent years, much effort has been put into producing efficient heat sink materials showing both a high conductivity and a low coefficient of thermal expansion (CTE) tunable to that of the material it has to cool down (Zweben, 1998, 2005, 2007). In particular, very high thermal conductivities have been achieved using diamond powder-based Metal Matrix Composites (MMC) with aluminium (Molina *et al*. 2008; Edtmaier *et al*. 2009), copper (Schubert *et al*. 2008a; Weber and Tavangar, 2007; Yoshida and Morigami, 2004) or silver (Tavangar *et al*., 2007; Weber and Tavangar 2009) as a matrix material. However, in the case of copper and silver and for production routes not including the sintering of diamonds, the adjunction of an element (e.g. B, Cr in Cu and Si in Ag) to the matrix metal is necessary to obtain the desired properties. Moreover, the obtained properties vary strongly as a function of the diamond particle size (Tavangar *et al*., 2007), an effect often observed in MMCs, for example (Kida *et al*., 2011). This effect can be attributed to a finite thermal conductance of the interfaces between the matrix metal and the dielectric reinforcement. This thermal boundary conductance (TBC), *G*, is equal to the ratio of heat flux across the interface, *J*, and the difference in temperature between either side of the interface, ΔT_{int}:

$$1. \quad G = \frac{J}{\Delta T_{int}}$$

in units of W/m²/K and can be used to determine an effective conductivity of the inclusions in MMCs involving the intrinsic thermal conductivity of the inclusions and their size. Composite properties can then be derived using the Maxwell Mean Field (Hasselman and Johnson, 1987) or the Differential Effective Medium models (Tavangar *et al*., 2007) based on this effective inclusion thermal conductivity. In the cases of Al/diamond (Beffort *et al*., 2006; Kleiner *et al*., 2006) and Cu(Cr)/diamond (Schubert *et al*., 2008a; Schubert *et al*. 2008b), the formation of isolated carbides or a carbide layer, respectively, at the interface between the matrix and the diamond has been observed and is suggested to be responsible for good thermal coupling between the matrix and the particles. For Cu-based diamond composites, the absence of such a coupling layer leads, typically, to very poor adhesion and low TBC. Therefore, efforts have been made to directly introduce an adhesion layer on a diamond surface via thin film deposition (Abyzov *et al*., 2011; Eisenmenger-Sittner *et al*., 2006; Hell *et al*., 2010; Schäfer *et al*., 2010; Schwarz *et al*., 2006) to improve the adhesion and/or TBC between diamond and the otherwise not adhering Cu matrix metal.

In this paper, time domain thermoreflectance (TDTR) is applied to directly measure the TBC between a metallic thin film and diamond with the anticipation to be able to assess the potential of this layer to serve as an adhesion layer between a Cu matrix and, thus, to

improve the conductance of a diamond-based MMC made using coated particles. Mo, Cr, Nb and W are used because they do have very limited solid solubility in, yet strong interface with, copper and form carbides with diamond, which is expected to happen when the MMC is produced. In this paper, the link between adhesion of a metallic layer on diamond and TBC between the former and the latter is emphasized. TDTR has long been used successfully to measure the TBC of interfaces in metal/metal (Clemens *et al*., 1988; Gundrum *et al*., 2005) or metal/dielectric systems (Hopkins *et al*., 2007; Hopkins *et al*. 2008; Lyeo and Cahill 2006; Stevens *et al*., 2005; Stoner and Maris 1993). This technique has the advantage to offer insight on nanometer-scale thermal diffusion effects, and thus is able to isolate the influence of a single interface on conductivity (Cahill *et al*., 2002, 2003). It takes advantage of the property of metals that their reflectivity varies linearly with small temperature variations (Ujihara, 1971). The main requirements and experimental stages to get precise measurements of TBC by TDTR in diamond-based systems will be described. This knowledge will then be applied to investigate the TBC between diamond and Cu, Mo, W, Nb and Cr and its evolution on heat treatment in vacuum.

2. Experimental details

2.1 Thermal boundary conductance measurement method

A schematic of the TDTR setup built in our laboratory is shown in Figure 1 and is similar to the one described in (Kang *et al*., 2008). A femtosecond laser beam, pulsed at 80 MHz, is split into two parts, the pump and the probe. The pump beam is modulated at 10·7 MHz using an electro-optic modulator (EOM) and then passes through a mechanical delay stage. The two beams are then focused on the same spot using a 10× microscope objective. The operation of the setup consists in recording the reflected intensity of the probe pulses due to the change in reflectance induced by the heating caused by the pump pulses as a function of the time delay between them, which is induced mechanically by changing the path length of the pump. Thus, a cooling curve of a metallic surface between 0 and 4 ns, after the heating of the metal surface by a pump pulse, with a precision down to the picosecond range can be measured. Since the recorded signal is low, passive frequency filtering, followed by preamplification and lock-in detection, at the frequency of the pump modulation is used to improve the signal to noise ratio. The obtained cooling curve is not only affected by the thermal properties of the surface material as well as the layers beneath it, but also by heat-accumulation effects due to the high repetition rate of the laser (Cahill 2004; Costescu *et al*., 2003; Schmidt *et al*., 2008). To further improve the reliability of the measurement, both the in-phase (X) and out-of-phase (Y) signals recorded by the lock-in amplifier are used. Indeed, they both depend in the same manner on artifacts due to variations in pump and probe spot overlap and thus the ratio X/Y is a more robust measurement than X alone (Costescu *et al*., 2003). Since the result is then a nontrivial function containing several parameters, an algorithm based on an analytical solution for

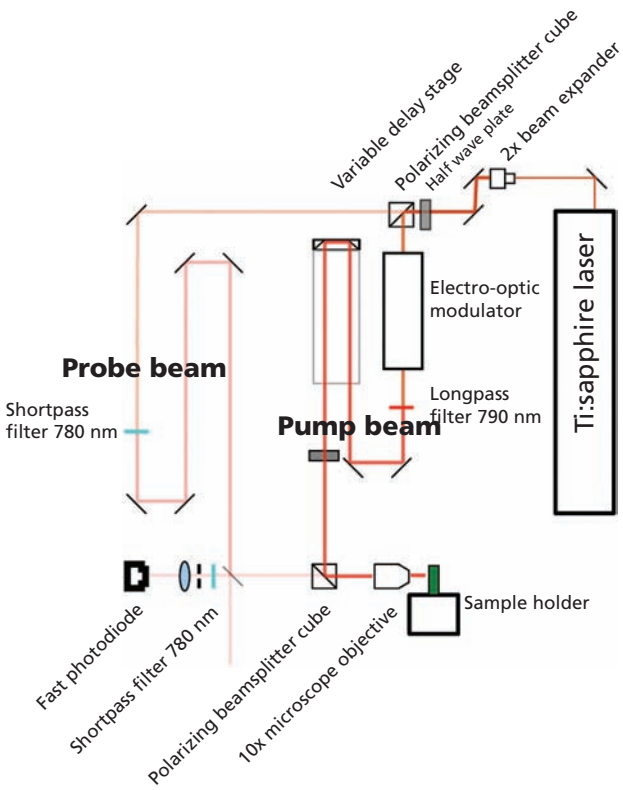

Figure 1. Schematics of the time domain thermoreflectance (TDTR) setup used in the TBC measurements presented. The laser repetition rate is 80 MHz and its wavelength is set at 785 nm to be able to work with 2 colors (one for the pump, one for the probe). The EOM modulation frequency is 10·7 MHz. The $1/e^2$ radius of the pump and probe beams is of approximately 7·4 μm and their power are set at 18 ± 1 mW (0·45 nJ per pulse / 0·26 mJ/cm^2) and 8 ± 0·5 mW (0·1 nJ per pulse / 0·06 mJ/cm^2).

heat flow in a layered system described in (Cahill 2004) is used to extract the TBC from the results.

2.2 Analysis of the sensitivity of TDTR simulations to free parameters

Given the ability of this model to accurately describe other thermal systems (Collins *et al*., 2010; Costescu *et al*., 2003; Gundrum *et al*., 2005; Hopkins *et al*., 2010a; Lyeo and Cahill 2006; Schmidt *et al*., 2010), it is used to investigate the sensitivity of the measurement in a model case of Cr on diamond. The sensitivity parameter is the same as described in (Costescu *et al*., 2003; Hopkins *et al*., 2010b), namely:

$$2. \qquad S_i = \frac{\delta \ln\left(-\frac{X}{Y}\right)}{\delta \ln(i)}$$

with *i* the parameter to be investigated. A value close to zero means that a parameter has a low influence and conversely, a value far from zero, no matter its sign, means that the parameter has a high influence. The diamond substrate is expected to have thermal properties that can be considered to be those of a semi-infinite, bulk solid in the investigated time scale and the heat capacity of a metallic thin film is not expected to vary with its thickness even at thicknesses well below the ones used in this work (Zhang *et al*., 2002). The critical unknown parameters are thus the exact film thickness, the film heat conductivity (known to be lower than the bulk value for thin films (Chen 2001, 2002; Feng *et al*., 2009) and the spot size of the pump and probe beams. First the sensitivities to the sample characteristics is calculated, namely to the metallic layer conductivity κ and thickness d. Since they are both (within limits) free parameters, in each case, the sensitivity for an array of the other parameter is calculated (i.e. $S\kappa$ for several d and conversely). The resulting curves are evaluated at a time well below (100 ps) and well above (2000 ps), the typical diffusion time in the layer given by d^2C_v/κ with C_v the volumetric heat capacity of the metal. Then the sensitivity to the laser spot size is calculated.

Figure 2 shows the results obtained for sensitivities to the layer thermal conductivity and thickness. The conductivity of bulk chromium of 93·7 W/m/K was taken from tables as the principal benchmark conductivity, and other conductivities ranging from 30 to 400 W/m/K were taken arbitrarily to cover the entire range of possible metal conductivities that can be expected from metallic thin films that are being investigated. The metal layer has a greater influence on the thermal model at 100 ps than at 2000 ps, especially when it is thicker and less conductive, and this does not vary much with G. At 2000 ps, the sensitivity to the thickness is substantially larger than that to the layer conductivity for the entire range of G except around 200 MW/m^2/K. Other simulations at 1000 and 4000 ps suggest that this point of reduced sensitivity to thickness varies with delay time and otherwise shows the same trends in shape and magnitude. It is therefore concluded that knowing precisely the metallic-layer thickness is a crucial point for this measurement, and, that, if only longer delay times are taken into account, layer conductivity has only a minor role in the signal change.

Figure 3 shows the measurement of sensitivity to the e^{-2} spot size of the pump and probe beams on the sample surface. It seems to be important at all G above 50 MW/m^2/K, and thus it also has to be known precisely.

2.3 Sample preparation and thickness characterization method

Samples consist of layers of about 100 nm in thickness of the metal to be investigated, deposited on diamond using a Balzers BAS 450

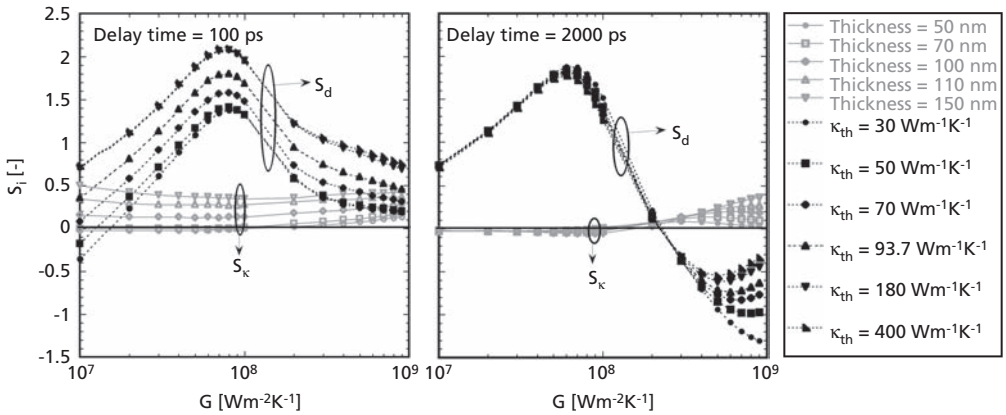

Figure 2. Sensitivity parameters calculated for the metallic layer conductivity κ and its thickness d. The lines are put as guide to the eye. Open grey symbols account for $S\kappa$, plain black symbols for S_d. The sensitivity of κ is calculated for a range of possible d and conversely. The conductivity of the layer is varied around 93·7 W/m^2/K (that of pure Cr) when calculating S_k. The thickness is varied around 90 nm when calculating S_d. The sensitivity values are given for a respectively short (100 ps) and long (2000 ps) delay time as compared to the typical diffusion time in the layer—about 300 ps. Curves plotted at 1000, 3000 and 4000 ps show the same trends as 2000 ps.

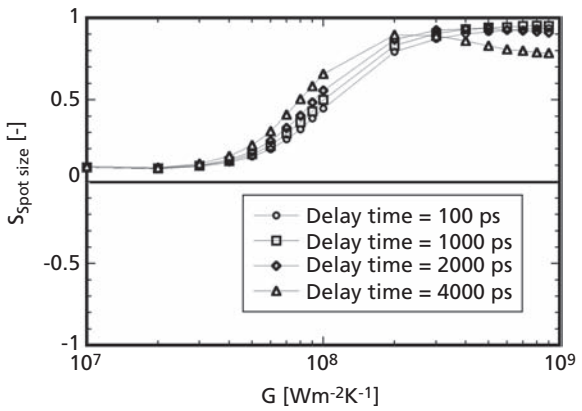

Figure 3. Sensitivity parameter calculation varying pump and probe the spot radius around 7·4 μm. The metallic layer consists in 90 nm of Cr with bulk conductivity value of 93·7 W/m/K and heat capacity of 3·3 MJ/m³/K.

DC magnetron sputter deposition machine. The sputtering gas is Ar, at a pressure of $5{\cdot}2 \times 10^{-3}$ mbar, and the power depends on the metal, ranging from 500 to 2000 W. Prior to deposition, the diamond samples (model MWS25 industrial diamond from the High Temperature High Pressure process, provided by Element 6, Shannon, Co. Clare, Ireland) are polished with diamond powders to 1 μm in size. Subsequently, they are first sonicated in acetone for 5 min, followed by sonication in ethanol for 2 min. They are finally rinsed using isopropanol. To deposit chromium, additional samples were prepared with an adhesion treatment of 15 min using an Ar:O plasma that was applied to the diamonds after polishing and rinsing because the adhesion of the layer on samples without plasma treatment was poor and complete decohesion could be observed on some specimens after heat treatment. The roughness of the diamonds could not be seen by FIB cross-section and therefore it is estimated to be less than 3 nm.

To measure the layer thicknesses (which are critical to our measurement, see Figure 2) in a repeatable and precise manner, a Zeiss NVision 500 Focused ion beam (FIB) system is used. A FIB system requires a calibration in the same way as a profilometer but has the advantage to give a good insight of the microstructure of the layer—for example, its homogeneity and fine surface roughness, and can be used at any point in the lifetime of the sample, including after a heat treatment that changes the layer chemical composition and thus its thickness. Another good method would be to use acoustic echos from TDTR signal (Stoner and Maris 1993; Thompsen *et al*., 1986), but it has two drawbacks that make an independent measurement useful in our view: (a) if the metallic layer is strongly textured, which is often the case, the speed of sound in it will take the value characteristic for the prominent crystallographic direction and hence may necessitate an additional texture analysis and (b) if the adhesion to the substrate is very strong and the change of acoustic impedance is low, acoustic echos are very difficult to detect due to high damping even of the first reflection at the metal/diamond interface (Tas *et al*., 1998). To measure thicknesses, FIB cross-sections in the sample were made and the resulting profile was measured by standard Scanning Electron Microscopy, for example, (Cheng *et al*., 2009). Corrections have to be made to account for the 54° angle between the electron and ion beam (Uchic *et al*., 2007). To do so, cross-section profiles are extracted and compared with simulation made with the CASINO software (Drouin *et al*., 2007).

Figure 4 shows a typical procedure used to measure a metallic layer thickness. Note that due to both the substantial difference in atomic densities between carbon and the metals and the angle of 36° at which the electron beam hits the interface, determination of the interface position is not straightforward. Indeed, for all the materials observed, it lies at the beginning of the upper plateau in the BSE signal indicating the metal layer for the carbon cap layer/metallic layer interface and at the beginning of the lower plateau indicating the diamond for the other interface.

3. Experiment

Beside the thickness uniformity and general aspect of the layers was investigated in the same FIB system. Some of the samples were heat treated up to 600°C in a vacuum of 10^{-7} mbar or better in an in-house vacuum annealing setup available at the Laboratory of Ceramics, EPFL. Thicknesses of the layers were measured before and after heat treatment. Due to the increase in volume on conversion of the metal layer into carbide, the formation of carbide can be assessed by measuring the change in thickness of the layer. The metallic-layer thicknesses measured after deposition and after heat treatment at 600°C are presented in Table 1. Significant changes in thickness are only observed in the cases of Cr and W. Since the transformation to carbide seemed to be complete in the case of Cr, two separate diamond samples with a 65 nm Cr layer were produced, one of which was heat treated in the same way as above and investigated by XPS in depth-profile mode.

To calibrate the beam spot size on the sample as well as possible, a first estimation of the spot size in focus was made using a 10 μm diameter pinhole and assuming Gaussian shape of the beam. Rounds of fits on samples exhibiting high G were then performed (to have a maximum sensitivity to the spot size), varying both G and the spot size, fitting the data as closely as possible at all times. A spot $1/e^2$ radius of 7·4 μm was obtained. Given an uncertainty of 0·8 μm on this value, due to the fact that the pinhole method may overestimate the size of the spot, a relative error of 8 % was calculated for high G cases based on the variation of G in the sensitivity analysis, cf. Equation 1. This possible error will be added to the uncertainty of the measured values.

Five measurements were made by TDTR on all samples in all obtained conditions (with and without annealing, and with a variation of the annealing temperature). The pump and probe beam

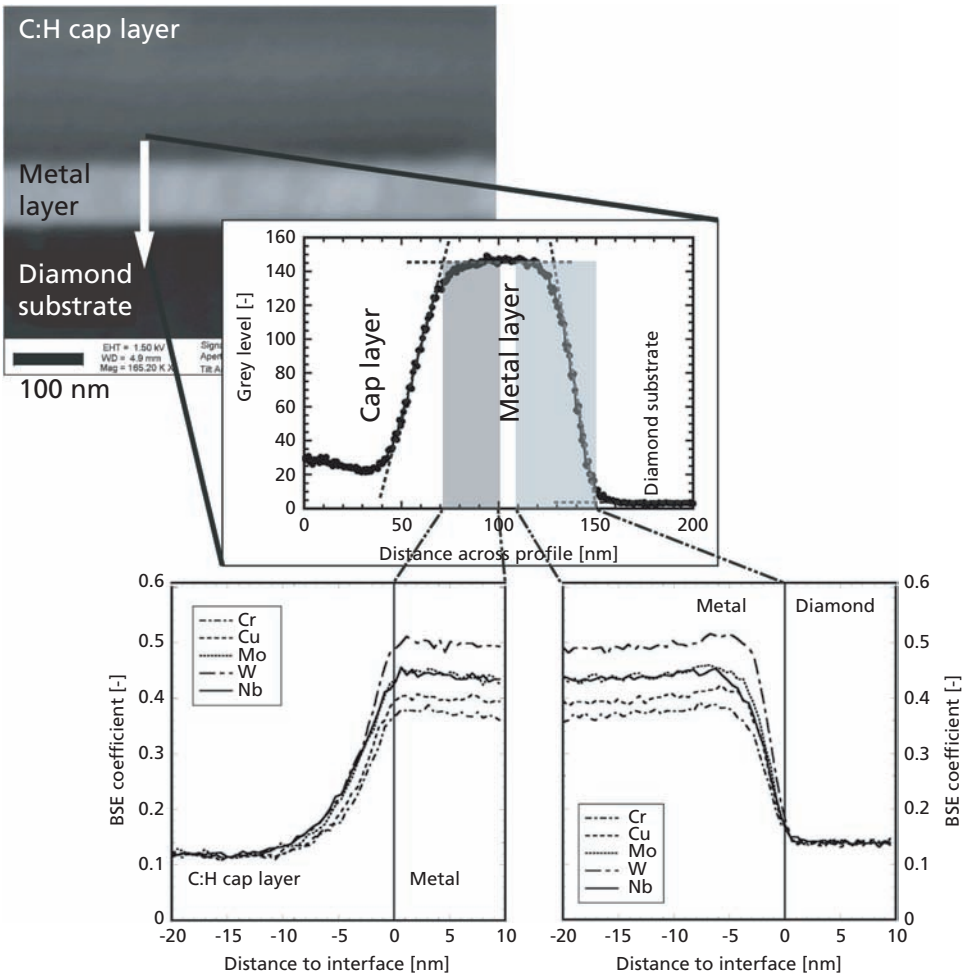

Figure 4. Example of thickness measurement from using FIB, with comparison to simulation. The exact location of the interface differs significantly from one interface to the other.

Metal	Initial thickness [nm]	Thickness after 600°C heat treatment [nm]	Potential thickness*[nm]	Carbide formation?	Proof
W	106 ± 3	117 ± 4	138 ± 4 (WC)	Partly	Thickness
Mo	97 ± 3	95 ± 3	110 ± 3 (Mo_2C)	No	Thickness
Nb	112 ± 3	112 ± 2 (Partial decohesion)	130 ± 3 (Nb_2C)	No	Thickness
Cr	75± 2	— (decohesion)	—	—	—
Cu	61 ± 2	61 ± 2	61 ± 2	No	No reaction possible
Cr:O:C	89 ± 3	98 ± 5	101 ± 3 (Cr_7C_3)	Yes	XPS, XRD

* The expected carbide (of which chemical composition is indicated in brackets) thickness if the metal has entirely reacted with the substrate on heat treatment. No stable carbide exists for copper.

Table 1. Metal films thicknesses measured by FIB before and after heat treatment in vacuum at 600°C for 2 hours. Also indicated is the expected carbide thickness if the metal has completely reacted with the substrate on heat treatment.

were maintained at 18 and 8 mW, respectively. The overall error due to the material properties and thickness is taken to be 4% and 3%, respectively.

4. Results

Figure 5 shows the results of XPS measurements on two Cr 65 nm on diamond samples, one of which received a vacuum annealing at 600°C for 2 hours. The signal is plotted versus the time of sputtering the sample surface with Ar. Only this system was investigated by this method because complete transformation to chromium carbide is suspected on annealing via thickness measurement.

Figure 6 shows the results for the TBC extracted from TDTR measurements. The samples denomination indicates, first, the layer element, then the thickness, the substrate element, and the sample number (i.e. Mo 97 nm C 2 means the second sample of a series of diamond samples with a 97 nm layer of molybdenum deposited on them). They are numbered to show the dispersion of the results between samples with the same treatment. Only one sample is shown for Cr, Cu and Nb because all the measurements yielded values within a 10% difference as compared to the one shown in each case. The best TBC measured in this study is that between Cr and an oxygen plasma-treated diamond surface and is of 325 ± 55 MW/m^2/K. In the only case where complete transformation of the Cr layer to Cr_7C_3 is suspected, as suggested by the XPS measurement in Figure 5 and the thickness measurement in Table 1, a Cr_7C_3/diamond interface is measured using thermal properties from (Pierson, 1996) to be of 350 ± 55 MW/m^2/K.

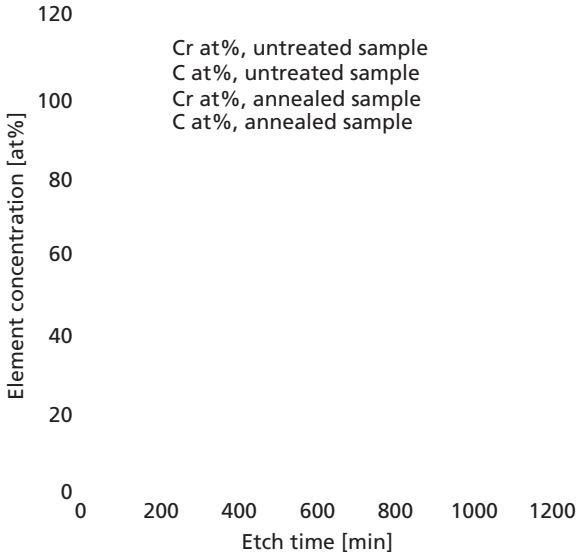

Figure 5. XPS depth profile of a diamond sample with a 65 nm Cr layer on top, with (filled symbols) and without (open symbols) a 600°C vacuum annealing for 2 hours. C and Cr are presented with squares and circles, respectively. A carburization of the chromium is suggested by an increased proportion of C atoms in the annealed sample.

Figure 7 shows a common feature observed among all the samples exhibiting a low TBC between metal and substrate, namely blisters indicating local decohesion between the layer and the substrate.

5. Discussion

The results in Figure 5 are only indicative of the actual composition of the Cr layer after annealing. Indeed, the depth profile involves a progressive sputtering of the layer with Ar atoms and the sputtering rate of Cr and C atoms may not be the same. Also, if the spot on which X-rays are incident does not lie exactly in the centre of the sputtered region, signal may be due to the carbon-rich surface, resulting in changing the measured proportions. In other metal/diamond couples, no change in thickness was observed indicating that either the layer has not reacted after the heat treatment or was already completely reacted after deposition. The fact that XRD measurements did not show any evidence of carbide formation is not a proof of their absence, since texture may account for this result as well. Further investigations by TEM are required to confirm the

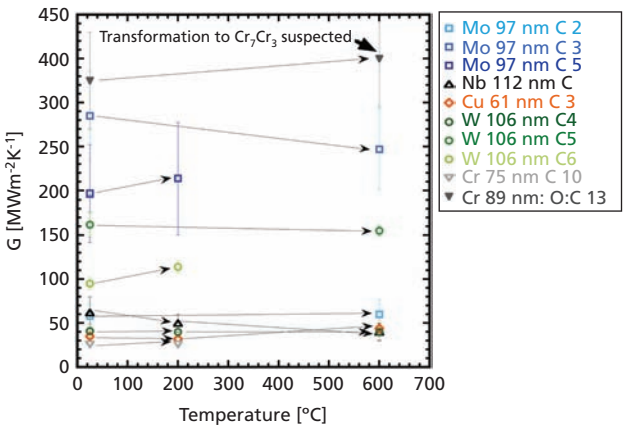

Figure 6. Results obtained for G as a function of isochronal (2 hours) annealing temperature for Molybdenum (Mo, open squares), tungsten (W, open circles), Niobium (Nb, upward oriented triangles), Copper (Cu, open diamonds) and Chromium (Cr downward oriented triangles) films deposited on diamond substrate by sputtering. When significant discrepancies were observed between several samples of the same couple, all the representative cases are shown. These representative case are denoted by the sample names in the legend on the top right. The error bars show the standard deviation over five measurements, plus the error on the other free parameters. The arrows are a guide to the eye to show that the same sample have been measured before and after heat treatment. On the top right of the graph is shown the TBC between Cr_7C_3 and diamond as complete transformation of the Cr layer to the former of the layer is suggested by XPS and thickness measurements.

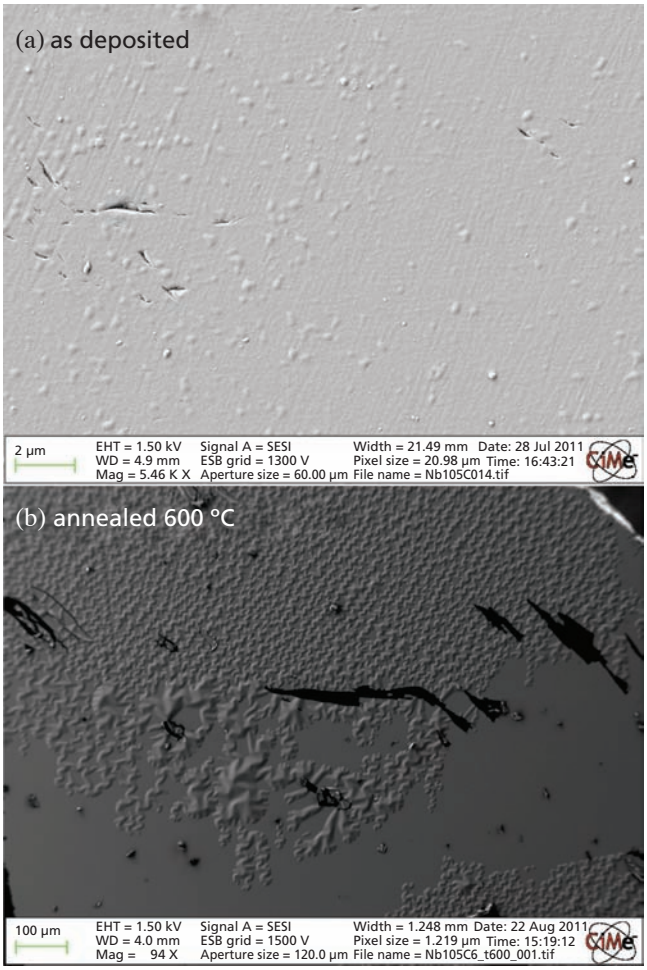

Figure 7. Scanning electron micrographs showing blisters observed in a 110 nm Nb film on diamond. These blisters were systematically observed in all the samples exhibiting a poor TBC between the metal and substrate. In case (a) the sample is as deposited. In case (b) it has been annealed at 600°C for 2 hours. The TDTR measurement made for this case were performed on the part still adhering to the substrate.

above assertions, but it is assumed that the Cr layer investigated in Figure 5, which corresponds, in terms of preparation conditions, to the one denoted as Cr 89 nm:O:C13 presented in Figure 6, has transformed into a chromium carbide after a 2-hour annealing at 600°C. The other layers are treated as metallic in the results and discussion.

Figure 6 shows that even for the same metallic film on substrates having received the same treatment, the TBC measured between the metal and the substrate can vary significantly. This result is also related to the observation of blisters in the film, indicating a biaxial compressive stress-relaxation mechanism (Hutchinson *et al.*, 1992). Since the films were deposited under the same conditions and thus the same stress is present initially in the film, the presence of blisters in the cases of low TBC and the quasi-absence of them in high TBC cases suggests that the adhesion is weaker in the former case. One possible explanation of this could be that there are still organic residues on the surface of the diamond and that they impede proper adhesion between layer and substrate. Another explanation would be that the species passivating the diamond surface differ from one sample to the other, for example, due to slight misorientations of the crystal. Indeed, the presence of hydrogen at a metal/diamond interface has already been observed to reduce substantially the TBC (Collins *et al.*, 2010; Lyeo and Cahill, 2006), its binding force (Guo *et al.*, 2010; Qi and Hector, 2003) as well as its electrical properties (Kageshima and Kasu, 2009) and the polishing process is expected to leave a mainly hydrogenated surface; but the hydrogen surface density changes with orientation (Kawarada, 1996). However, the presence of oxygen seems to be beneficial (Collins *et al.*, 2010) and is known to change significantly other interfacial properties, for example, work function (Gamo *et al.*, 2007a, 2007b) and electronic properties (Mori *et al.*, 1991; Zheng *et al.*, 2001). Moreover, the binding force at the interface has already been suggested to change the TBC at interfaces when transfer is governed by phonons (Prasher, 2009; Stoner and Maris, 1993; Young and Maris, 1989).

Figure 6 also suggests that if the TBC between a metallic layer and diamond is poor in the first place, a subsequent heat treatment up to 600°C for 2 hours does not change dramatically the TBC. Moreover, annealing can lead to more serious decohesion phenomena such as the telephone-cord buckling (Hutchinson *et al.*, 1992; Moon *et al.*, 2002) observed in Figure 7 b) or even complete decohesion. This result suggests that if the binding is poor, the passage of C atoms through the interface to form carbides on annealing is strongly reduced, which would explain the absence of a change in layer thickness as shown in most samples (except for W:C and Cr:O:C) in Table 1. Conversely, to have a good TBC between a carbide and diamond, the TBC has to be good before annealing the sample. To test this hypothesis, the diamond samples in an Ar:O plasma for 15 minutes before depositing a 89 nm layer of Cr on them is used (last sample in Table 1, sample Cr 89 nm:O:C on Figure 6), as mentioned in the earlier section on samples. The resulting measured TBC between Cr and diamond is 325 ± 55 and 300 ± 50 MW/m^2/K. These values are a factor of 11 higher than the ones acquired for Cr without plasma treatment as well as the other samples considered in this study. Moreover, practically no blisters could be found in the metal film, suggesting an improved adhesion. After heat treatment of one of the samples at 600°C for 2 hours and assuming complete transformation (see Figure 5) into a Cr_7C_3 phase, a Cr_7C_3/diamond interface is measured to be 350 ± 55 MW/m^2/K. This last result remains preliminary until a complete investigation is performed by TEM to identify the exact phase/s contained in the sample.

6. Conclusions

The experimental setup and technique of time domain thermoreflectance (TDTR) has been presented and its potential to

assess potential routes to improve the thermal coupling between diamond and copper using mediating metallic thin films has been discussed. Using an analytical solution of the thermal problem, it is found that the free parameters most strongly governing the measurement are the spot size and the metallic-layer thickness. Results for Cu, Cr, Nb, W and Mo on diamond are presented, and the importance of layer adhesion is highlighted since bad adhesion leads to blistering, low TBC and seems to prevent carbide formation on annealing of the sample. Moreover, after an Ar:O plasma treatment with the purpose to improve adhesion, the thermal conductance between a Cr layer sputtered in the same conditions as samples prepared without this treatment exhibited a maximum TBC between Cr and diamond of 325 ± 55 MW/m^2/K, a factor of 11 higher than the latter. After annealing at 600°C for 2 hours, XPS measurement suggested a transformation of the Cr in carbide, presumably Cr_7C_3, leading to the measurement of a TBC between this carbide and diamond of 350 ± 55 MW/m^2/K. Therefore, to improve the TBC between copper and diamond using mediating metallic thin films, good adhesion of the thin films has to be obtained even before carbide formation.

Acknowledgments

Financial support of C. Monachon by the SNSF Project No. 200021-121881 is gratefully acknowledged. The authors are also grateful to P. Muralt and M. Iwanowska at the Ceramics Laboratory of EPFL for vacuum annealing bench and to M. Cantoni and P. Burdet at the Interdisciplinary Center for Electron Microscopy CIME at EPFL for their help and useful discussions concerning the FIB analysis. In the same laboratory, the authors kindly acknowledge V. Laporte and N. Xanthopoulos for the XPS analysis of their samples. Finally, Professor Hubert Girault of the Laboratoire d'Électrochimie Physique et Analytique LEPA at EPFL is acknowledged for providing the laser source for the experiments. Prof David G. Cahill of University of Illinois at Urbana Champaign is gratefully acknowledged for helpful discussions.

REFERENCES

Abyzov AM, Kidalov SV and Shakhov FM (2011) High thermal conductivity composites consisting of diamond filler with tungsten coating and copper (silver)matrix. *Journal of Materials Science* **46**: 1424–1438.

Beffort O, Khalid FA, Weber L *et al.* (2006) Interface formation in infiltrated Al(Si)/diamond composites. *Diamond and Related Materials* **15**: 1250–1260.

Cahill DG (2004) Analysis of heat flow in layered structures for time-domain thermoreflectance. *Review of Scientific Instruments* **75**: 5119–5122.

Cahill DG, Goodson KE and Majumdar A (2002) Thermometry and thermal transport in micro/nanoscale solid-state devices and structures. *Journal of Heat Transfer* **124**: 223–241.

Cahill DG, Wayne FK, Goodson KE *et al.* (2003) Nanoscale thermal transport. *Applied Physics Reviews* **93**: 793–818.

(2001) Ballistic-diffusive heat-conduction equations. *Physical Review Letters* **86**: 2297–2300.

Chen G (2002) Ballistic-diffusive equations for transient heat conduction from nano to macroscales. *Journal of Heat Transfer* **124**: 320–328.

Cheng J, Perrie W, Sharp M *et al.* (2009) Single-pulse drilling study of Au, Al and Ti alloy by using picosecond laser. *Applied Physics A* **95**: 739–746.

Clemens BM, Eesley GL and Paddock CA (1988) Time-resolved thermal transport in compositionally modulated metal films. *Physical Review. B, Condensed Matter* **37**: 1085–1096.

Collins KC, Chen S and Chen G. (2010) Effects of surface chermistry on thermal conductance at aluminum-diamond interfaces. *Applied Physics Letters* **97**: 1–3.

Costescu RM, Wall MA and Cahill DG. (2003) Thermal conductance of epitaxial interfaces. *Physical Review B* **67**: 1–5.

Drouin D, Couture AR, Joly D *et al.* (2007) CASINO V2.42: a fast and easy-to-use modeling tool for scanning electron microscopy and microanalysis users. *Scanning* **29**: 92–101.

Edtmaier C, Weber L and Tavangar R (2009) Surface modification of diamonds in diamond/Al-matrix composite. *Advanced Materials Research* **59**: 125–130.

Eisenmenger-Sittner C, Schrank C, Neubauer E *et al.* (2006) Modification of wetting of copper (Cu) on carbon (C) by plasma treatment and molybdenum (Mo) interlayers. *Applied Surface Science* **252**: 5343–5346.

Feng B, Li Z and Zhang X. (2009) Prediction of size effect on thermal conductivity of nanoscale metallic films. *Thin Solid Films* **517**: 2803–2807.

Gamo H, Gamo MN, Nakagawa K and Ando T (2007a) Surface potential change by oxidation of the chemical vapor deposited diamond (001) surface. *Journal of Physics: Conference Series* **61**: 327–331.

Gamo H, Iwasaki K, Nakagawa K, Ando T and Gamo MN (2007b) Surface conductivity change by oxidation of the homoepitaxially grown diamond (100) surface. *Journal of Physics: Conference Series* **61**: 332–335.

Gundrum BC, Cahill DG and Averback RS (2005) Thermal conductance of metal-metal interfaces. *Physical Review B* **72**: 1–5.

Guo H, Qi Y and Li X (2010) Adhesion at diamond/metal interfaces: A density funcitonal theory study. *Journal of Applied Physics* **107**: 1–8.

Hasselman DPH and Johnson LF (1987) Effective thermal conductivity of composites with interfacial thermal barrier resistance. *Journal of Composite Materials* **21**: 508–515.

Hell J, Horkel M, Neubauer E and Eisenmenger-Sittner C (2010) Construction and characterization of a sputter deposition system for coating granular materials. *Vacuum* **84**: 453–457.

Hopkins PE, Norris PM and Stevens RJ (2008) Influence of inelastic scattering at metal-dielectric interfaces. *Journal of Heat Transfer* **130**: 1–9.

Hopkins PE, Phinney LM, Serrano JR *et al*. (2010a) Effects of surface roughness and oxide layer on the thermal boundary conductance at aluminum/silicon interfaces. *Physical Review B* **82**: 1–5.

Hopkins PE, Salaway RN, Stevens RJ and Norris PM (2007) Temperature-dependent thermal boundary conductance at Al/Al2O3 ant Pt/Al2O3 interfaces. *International Journal of Thermophysics* **28**: 947–957.

Hopkins PE, Serrano JR, Phinney LM *et al*. (2010b) Criteria for cross-plane dominated thermal transport in multilayer thin film systems during modulated laser heating. *Journal of Heat Transfer* **132**: 1–10.

Hutchinson JW, Thouless MD and Liniger EG (1992) Growth and configurational stability of circular, buckling-driven film delamination. *Acta Metallurgica Materialia* **40**: 295–308.

Kageshima H and Kasu M (2009) Origin of Schottky barrier modification by hydrogen on diamond. *Japanese Journal of Applied Physics* **48**: 1–5.

Kang K, Koh YK, Chiritescu C, Zheng X and Cahill DG (2008) Two-tint pump-probe measurements using a femtosecond laser oscillator and sharp-edged optical filters. *Review of Scientific Instruments* **79**: 114901.

Kawarada H (1996) Hydrogen-terminated diamond surfaces and interfaces. *Surface Science Reports* **26**: 205–259.

Kida M, Weber L, Monachon C *et al*. (2011) Thermal conductivity and interfacial conductance of AlN particle reinforced metal matrix composites. *Journal of Applied Physics* **109**: 1–8.

Kleiner S, Khalid FA, Ruch PW, Meier S and Beffort O (2006) Effect of diamond crystallographic orientation on dissolution and carbide formation in contact with liquid aluminium. *Scripta Materialia* **55**: 291–294.

Lyeo HK and Cahill DG (2006) Thermal conductance of interfaces between highly dissimilar materials. *Physical Review B* **73**: 144301–144306.

Molina JM, Rhême M, Carron J and Weber L (2008). Thermal conductivity of aluminum matrix composites reinforced with mixtures of diamond and SiC particles. *Scripta Materialia* **58**: 393–396.

Moon MW, Jensen HM, Hutchinson JW, Oh KH and Evans AG (2002) The charcterization of telephone cord buckling of compressed thin films on substrates. *Journal of the Mechanics and Physics of Solids* **50**: 2355–2377.

Mori Y, Kawarada H and Hiraki A (1991). Properties of metal/diamond interfaces and effects of oxygen adsorbed onto diamond surface. *Applied Physics Letters* **58**: 940–941.

Pierson HO (1996) *Handbook of Refractory Carbides and Nitrides*. Westwood, Noyes Publications.

Prasher RS (2009) Accoustic mismatch model for thermal contact resistance of van des Waals contacts. *Applied Physics Letters* **94**: 1.

Qi Y and Hector LG (2003) Hydrogen effect on adhesion and adhesive transer at aluminum/diamond interfaces. *Physical Review B* **68**: 1.

Schäfer D, Hell J, Eisenmenger-Sittner C *et al*. (2010) Suppression of de-wetting of copper coatings on carbon substrates by metal (Cr, Mo, Ti) doped boron interlayers. *Vacuum* **84**: 202–204.

Schmidt AJ, Chen X and Chen G (2008) Pulse accumulation, radial heat conduction, and anisotropic thermal conductivity in pump-probe transient thermoreflectance. Review of Scientific Instruments 79: 114902.

Schmidt AJ, Collins KC, Minnich A and Chen G (2010) Thermal conductance and phonon transmissivity of metal-graphite interfaces. *Journal of Applied Physics* **107**: 1–5.

Schubert T, Ciupinski L, Zielinski W *et al*. (2008a) Interfacial characterization of Cu/diamond composites prepared by powder metallurgy for heat sink applications. *Scripta Materialia* **58**: 263–266.

Schubert T, Trinidade B, Weisgarber T *et al*. (2008b) Interfacial design of Cu-based composites prepared by powder metallurgy for heat sink applications. *Material Science and Engineering A* **475**: 39–44.

Schwarz B, Schrank C, Eisenmenger-Sittner C *et al*. (2006) Molybdenum interlayers as adhesion promotors for thin copper films on plasma treated glassy carbon. *Surface and Coatings Technology* **200**: 4891–4896.

Stevens RJ, Smith AN and Norris PM (2005) Measurement of thermal boundary conductance of a series of metal-dielectric interfaces by the transient thermoreflectance technique. *Journal of Heat Transfer* **127**: 315–322.

Stoner RJ and Maris HJ (1993) Kapitza conductance and heat flow between solids at temperatures from 50 to 300 K. Physical Review. B, Condensed Matter 48: 16373–16387.

Tas G, Loomis JJ, Maris HJ *et al*. (1998) Picosecond ultrasonics study of the modification of interfacial bonding by ion implantation. *Applied Physics Letters* **72**: 2235–2237.

Tavangar R, Molina JM and Weber L (2007) Assessing predictive schemes for thermal conductivity against diamond-reinforced silver matrix composites at intermediate phase contrast. *Scripta Materialia* **56**: 357–360.

Thompsen C, Grahn H, Maris HJ and Tuac J (1986) Surface generation and detection of phonons by picosecond light pulses. *Physical Review B* **34**: 4229–4138.

Uchic MD, Holzer L, Inkson BJ, Principe EL and Munroe P (2007) Three-dimensional microstructural characterizazion using focused ion beam tomography. *MRS Bulletin* **32**: 408–416.

Ujihara K (1971) Reflectivity of metals at high temperatures. *Journal of Applied Physics* **43**: 2376–2383.

Weber L and Tavangar R (2007) On the influence of active element content on the thermal conductivity and thermal expansion of Cu-X (X = Cr, B) diamond composites. *Scripta Materialia* **57**: 988–991.

Weber L and Tavangar R (2009) Diamond-based metal matrix composites for thermal management made by liquid metal

infiltration—potential and limits. *Advanced Materials Research* **59**: 111–115.

Yoshida K and Morigami H (2004) Thermal properties of diamond/copper composite material. *Microelectronics Reliability* **44**: 303–308.

Young DA and Maris HJ (1989) Lattice-dynamical calculation of the Kapitza resistance between fcc lattices. Physical Review. B, Condensed Matter **40**: 3685–3693.

Zhang M, Efremov MY, Yu M *et al*. (2002) Real-time heat capacity Measurment during thin-film deposition by scanning nanocalorimetry. *Applied Physics Letters* **81**: 3801–3803.

Zheng JC, Xie XN, Wee ATS and Loh KP (2001) Oxygen-induced surface state on diamond (100). *Diamond and Related Materials* **10**: 500–505.

Zweben C (2007) Advances in high-performance thermal management materials—a review. *Journal of Advanced Materials* **39**: 3–10.

Zweben C (2005) Advanced electronic packaging materials. *Advanced Materials and Processes* **163**: 33–37.

Zweben C. (1998) Advances in composite materials for thermal management in electronic packaging *Journal of Managemnet* **50**: 47–51.